

Catalysis Science & Technology

Accepted Manuscript



This is an *Accepted Manuscript*, which has been through the Royal Society of Chemistry peer review process and has been accepted for publication.

Accepted Manuscripts are published online shortly after acceptance, before technical editing, formatting and proof reading. Using this free service, authors can make their results available to the community, in citable form, before we publish the edited article. We will replace this *Accepted Manuscript* with the edited and formatted *Advance Article* as soon as it is available.

You can find more information about *Accepted Manuscripts* in the [Information for Authors](#).

Please note that technical editing may introduce minor changes to the text and/or graphics, which may alter content. The journal's standard [Terms & Conditions](#) and the [Ethical guidelines](#) still apply. In no event shall the Royal Society of Chemistry be held responsible for any errors or omissions in this *Accepted Manuscript* or any consequences arising from the use of any information it contains.

Enhanced Low Temperature CO Oxidation by Pretreatment: Specialty of the Au-Co₃O₄ Oxide Interfacial Structures

Cite this: DOI: 10.1039/x0xx00000x

Received 00th January 2012,

Accepted 00th January 2012

DOI: 10.1039/x0xx00000x

www.rsc.org/

Y. Yao,^a L. L. Gu,^a W. Jiang,^a H. C. Sun,^a Q. Su,^a J. Zhao,^a W. J. Ji,^{*a} and C. T. Au^{*b}

In this study, the morphologically uniform Co₃O₄ cubes (*c*-Co₃O₄), hexagonal plates (*h*-Co₃O₄) and tetrakaidecahedrons (*t*-Co₃O₄) were carefully synthesized and the crystalline facets of (001), (111), and (112) were identified. Precise Au nanoparticles (3.1-3.3 nm) deposition on the three Co₃O₄ entities was achieved to obtain the specific Au-Co₃O₄ interfaces. A detailed comparison was made on the basis of their unique interfacial structures and catalytic behaviors. The H₂-TPR and XPS investigations revealed the important variations in reactivity of surface oxygen, surface Co³⁺/Co²⁺ ratio, evolution of surface oxygen vacant sites as well as Au oxidation state upon Au loading and pretreatments. The enhanced CO oxidation by Au deposition and particularly He- and in situ-pretreatments has been elucidated in light of the structural specialties associated with the three facets of Co₃O₄ substrates and the corresponding Au-Co₃O₄ interfaces. The consequence in activity enhancement for Co₃O₄ substrate and Au-Co₃O₄ interface is verified: (001) > (112) > (111), and Au/(112) > Au/(001) > Au/(111). The results of Au/*h*-Co₃O₄ also suggest that both Au cluster and Co₃O₄ structural feature can have a profound effect on the catalytic behaviour of generated interface. The present work extended the insights into the interface-dependent CO oxidation over the controllably prepared Au-Co₃O₄ interfacial structures.

Introduction

In recent years the certain nanostructures with specific morphologies and exposed crystal facets have been carefully fabricated, demonstrating significantly different behaviors in various reactions¹⁻⁶. The supported metal catalyst is one of the most important types of catalyst^{7a}. On the side of support, constitution, crystalline structure, specific surface area, texture and porosity are the important aspects to be considered; while on the side of loaded metals, sort of metal (especially Au), particle size and morphology, and metal-support interaction are also extensively explored^{7b}. Since the oxide support is generally in poly-crystalline state without controllable synthesis, the dispersion of metal particles on support surface is highly random, and the generated metal-support interaction is actually an average of those contributed by various metal-oxide interfaces which are structurally non-uniform, especially on the oxide surface side. And because of the complexity of metal-support interfaces, understanding the nature of metal-support interaction is therefore rather challenging.

The development in synthesis of nanomaterials has provided opportunities to gain deeper insights into the metal-support interactions. Controllable synthesis of differently

shaped nanocrystals with uniformly structural facets under nanoscale is considered to be an important prerequisite for studying the nature of different surfaces and/or interfaces with respect to their catalytic properties⁸⁻¹³. Through an effectively controllable synthesis, oxide nanoparticles (NPs) with certain dimension and morphology can be obtained. The facets of oxide support can be directly observed and identified by means of high resolution transmission electron microscopy (HRTEM). Laying on this recognition, different interfacial structures can be assembled upon careful deposition of metal particles onto the regularly-shaped metal oxide substrates. Since the facet structure of oxide support is distinguishable, the specific interface between metal and oxide facet can be compared in detail. This would be helpful for understanding the true metal-support interaction as well as the related catalytic mechanism. For CO oxidation it is well accepted that the catalytic performance is very sensitive to Au particle size, sort of support, preparation history, pre-treatment, and reaction condition. Au particles of different dimension and oxidation state were observed to function directly to the reaction, meanwhile the importance of Au-oxide interface was also proposed¹⁴⁻²³. Recently Kung and co-workers²⁴ reviewed the Au-metal oxide

support interface as catalytic active sites for three reactions: CO oxidation, water gas shift reaction, and selective oxidation of propane. Although many studies focused on the role of particle size and electron density of Au clusters, there is a trend to shift attention to the function of Au-oxide boundary/interface. Carley et al.²⁵ studied CO oxidation on Au/Fe₂O₃ by applying isotope labelling and density functional theory (DFT) and found that oxygen molecules can dissociatively co-adsorb with CO on the boundary Au atoms where oxidation undergoes. Kotobuki et al.²⁶ studied CO oxidation over Au/TiO₂ containing different sized Au NPs. It was demonstrated that the generated CO₂ is closely related to the Au-TiO₂ boundary length. A recent review given by Haruta²⁷ proposed a general mechanism of CO oxidation, considering the interfacial sites at which CO adsorbs on coordinately unsaturated Au atoms while oxygen adsorbs at the Au-support interface.

Cobalt oxide has received great attention due to its unique property in the applications of gas sensing, lithium-ion batteries, and catalysis²⁸⁻³⁵. Liotta et al.³⁶ provided a comprehensive review of the state-of-the-art researches that focus on the synthesis, structural properties and catalytic applications of Co₃O₄ nanocrystals and Co₃O₄-MO_x binary oxides in CO, CH₄, and VOC oxidation at low temperatures. Hu et al.⁶ early reported controllable synthesis of Co₃O₄ via a hydrothermal process, and found that the high indexed (112) crystal planes of Co₃O₄ NCs are more reactive than the (001) and (011) planes. Xie et al.¹¹ reported that the unique Co₃O₄ nanorods were able to catalyze CO oxidation at a temperature as low as -77 °C. It was demonstrated that the Co₃O₄ nanorods predominantly exposed the (110) planes, favoring the presence of active Co³⁺ species at the surface. These examples indicated that morphology control in synthesis of transition metal oxides is significant as highly efficient oxidation catalysts. Wang et al.³⁷ reported the nanoscale Co-based catalysts derived by simple thermolysis of a Co-containing metal-organic framework (ZIF-67) for low temperature CO oxidation. A catalyst obtained from ZIF-67 pyrolysis at 600 °C exhibited high activity and good durability. Kouotou et al.³⁸ studied CO oxidation on the spinel-type Co-Fe oxides where the reaction underwent by CO with surface adsorbed oxygen. Li et al.³⁹ prepared Co₃O₄ catalysts supported on TiO₂ with different crystalline phases (anatase, rutile and P25) for low-temperature CO oxidation. The Co₃O₄/TiO₂ (anatase) exhibited the highest activity mainly due to its highly defective structure and good oxygen adsorption ability. Teng et al.⁴⁰ synthesized the Co₃O₄ nanocrystals of different shapes (plates, rods, cubes, and spheres) and measured their catalytic activities for CO oxidation in dry reactant gas. The plate-like nanocrystals mainly exposing the (111) plane showed the highest catalytic activity.

Among differently shaped Co₃O₄ nanostructures, the form of nanocube is an interesting illustration which represents the dominantly exposed (001) crystal planes, ideal for studying crystal facet dependent properties⁴¹. Axel et al.⁴² observed that small sized Co₃O₄ cubes can be received by employing the agent of cetyltrimethylammonium bromide (CTAB); on the

other hand, large sized Co₃O₄ cubes will be produced via addition of benzylpyridine (BPy) in the preparation medium. Chen et al.⁴³ reported a poly-vinylpyrrolidone (PVP)-mediated hydrothermal method to synthesize well-crystallized Co₃O₄ cubes with an average edge length of ca. 350 nm.

For low-temperature CO oxidation, an interesting phenomenon has been recognized by different researchers. Park and Lee⁴⁴ observed that the rate of CO oxidation can change obviously over Au/TiO₂ with different pretreatment history: the pre-oxidized one is the most active; the inertly pretreated one is somehow less active; while the hydrogen pre-reduced one is the least active. Nie et al.^{45a} reported that oxygen pretreatment of Au₂₅(SR)₁₈ nanoclusters supported on CeO₂, TiO₂, and Fe₂O₃ at 150 °C resulted in a notable enhancement in CO oxidation activity; while Wang et al.^{45b} found that Au/α-Mn₂O₃ pretreated in helium exhibited higher activity for CO oxidation than the one pretreated in O₂ or H₂. Haruta and co-workers⁴⁶ systematically investigated the effects of pretreatment atmosphere, temperature, and moisture on CO oxidation activity of Co₃O₄, MnO₂, and NiO calcined at 300 or 400°C. It was demonstrated that the pre-treatment conditions do have profound influences on activity. Our recent studies extended these observations. The hollow structured Au/Fe₂O₃ obtained via a hybrid Au/β-FeOOH@SiO₂ precursor showed a significant enhancement in CO oxidation activity when in situ pre-treated at 180°C⁴⁷. The Co₃O₄ spheroids of different textures and the corresponding Au-loaded samples also encountered substantial enhancement in CO oxidation by in situ pretreatment⁴⁸. Note that in the above-mentioned systems the oxides themselves are essentially poly-crystallites or in amorphous state; and the Au/oxide interfaces are not controllably prepared.

The aim of this study is therefore motivated by the following two aspects: on one hand, the morphologically uniform Co₃O₄ cubes (*c*-Co₃O₄), hexagonal plates (*h*-Co₃O₄) and tetrakaidecahedron (*t*-Co₃O₄) were firstly synthesized, and then precious Au deposition with a narrow particle size distribution was achieved on these well-crystallized Co₃O₄ entities to obtain the unique interfaces between the Au NPs and the specific facets of Co₃O₄. On the other hand, pre-treatments of these interfacial structures were systematically conducted in inert (He) or reactive (in-situ) atmosphere. The catalytic behaviors can then be compared with respect to their certain active interfaces, to elucidate the origin and extent of pretreatment effect on different Au/facet interfaces. The results provided new insights into the significance of certain Au/facet structure (both Au entity and Co₃O₄ substrate) determining the activity of low temperature CO oxidation especially when the corresponding Au/facet structures experienced different pre-treatments.

Experimental

Catalyst preparation

Synthesis of β -Co(OH)₂ precursor: In a typical procedure, Cobalt chloride hexahydrate (CoCl₂·6H₂O) of 1.78 g was dissolved in 25 ml distilled water in a three-necked flask under a N₂ flow (30 ml min⁻¹). After the cobalt chloride was fully dissolved, NaOH of 0.025 mole was dissolved in 10 ml water to make a solution which was added drop wise by employing a constant pressure drop funnel. The liquid phase was continuously stirred by a magnetic stirrer. The mixture was transferred into a 50 ml Teflon-lined stainless steel autoclave, and subjected to a hydrothermal treatment at 180 °C for 24 h. After the autoclave was cooled down to room temperature (RT), the precipitate was collected and washed repeatedly with distilled water via centrifugation.

Synthesis of Co₃O₄ hexagonal plates (*h*-Co₃O₄): Air-calcination of β -Co(OH)₂ precursor was performed at 400 °C for 3 h.

Synthesis of Co₃O₄ cubes (*c*-Co₃O₄): PVP of 0.2 g was dissolved in a solution containing distilled water and concentrated ammonium hydroxide solution (v/v=1:1). After the PVP component was dissolved, Co(NO₃)₂ of 2.18 g was added into the solution under stirring. The mixture was transformed into a 250 ml Teflon-lined stainless steel autoclave, and subjected to a hydrothermal treatment at 180 °C for 6 h. After the autoclave was cooled down to RT, the precipitate was collected and washed repeatedly with distilled water via centrifugation. The sample was then calcined in air at 400 °C for 3 h.

Synthesis of Co₃O₄ tetrakaidecahedrons (*t*-Co₃O₄): PVP of 0.2 g was dissolved in a solution containing distilled water and concentrated ammonium hydroxide solution (v/v=1:1). After the PVP component was dissolved, Co(NO₃)₂ of 1.46 g was added into the solution under stirring. The mixture was transformed into a 250 ml Teflon-lined stainless steel autoclave, and subjected to a hydrothermal treatment at 180 °C for 12 h. After the autoclave was cooled down to RT, the precipitate was collected and washed repeatedly with distilled water via centrifugation. The sample was then calcined in air at 400 °C for 3 h.

Preparation of Au-loaded samples: Deposition-precipitation method was employed to load Au species on various Co₃O₄ substrates. Certain amount of Co₃O₄ was dispersed in distilled water, and then a HAuCl₄·3H₂O solution (0.0082 M) was added slowly with a nominal Au loading being 3% by weight. The pH of the suspension was adjusted by using a diluted ammonium solution till its value reached 9. After that, the mixture was put into a water bath kept at 50 °C and was continuously stirred for 3h. The product was collected by centrifugation and dried at RT overnight. The dried sample was further calcined at 250 °C for 2 h. The Au content measured by ICP-AES is 2.63-2.69 wt% for the three Au-loaded samples.

Materials characterization

X-ray diffraction (XRD) measurements were conducted on a Philips X'Pert MPD Pro X-ray diffractometer with Cu K α radiation ($\lambda = 0.1541$ nm). Elemental analysis of Au was

performed using ICP-AES on a J-A1100 Versa Probe spectrometer. The samples were dissolved in a mixture of concentrated HCl and HNO₃ with a volumetric ratio of 3:1 prior to analysis. The TEM images were taken over a JEOL JEM-1010 microscopy operated at 100 kV. The HRTEM images were taken on a JEOL JEM-2010 microscopy operated at 200 kV. To determine the particle size distribution of Au NPs on different Co₃O₄ substrates, at least 80 randomly distributed Au particles in different TEM images were measured and counted. N₂ sorption measurements were performed on a NOVA-2020 Material Physical Structure Determinator. Before measurement, samples were degassed at 300 °C for 4 h. BET surface areas were calculated based on a multipoint BET analysis of the nitrogen adsorption isotherms. Hydrogen temperature-programmed reduction (H₂-TPR) was carried out using a U-shaped quartz reactor. The catalyst (100 mg) was first pretreated in a He stream (50 ml min⁻¹) at 120 °C for 1 h. After the temperature was cooled down to RT, the sample was then heated to 700 °C at a rate of 10 °C min⁻¹ in a 5% H₂-Ar flow (50 ml min⁻¹), and the effluent gas was analysed using a TCD. X-ray photoelectron spectroscopy (XPS) analysis was performed on a PHI 5000 Versaprobe system, using monochromatic Al K α radiation (1486.6 eV) operating at 25 W. The sample was degassed overnight at RT in a UHV chamber (< 5×10⁻⁷ Pa). All binding energies (BEs) were referenced to the C1s peak at 284.6 eV. The raw spectra had been smoothed by averaging every three adjacent points once, and this treatment was typically applied to most routine analysis. The applied smoothing is light-weighted and has minor effect on the spectral features. The curve-fitting of the XPS spectra is done by employing XPS Peak 41 software which is widely applied. Due to the inelastic scattering of electrons, the XPS spectral peaks could be considerably distorted with a characteristic tail on the low-kinetic-energy side. To subtract the inelastic background for peak area determination, a number of empirical approaches have been employed, for instance, subtracting a linear type⁴⁹, a Shirley type⁵⁰, or a Tougaard type background⁵¹ is a general opinion. In the present study, the Shirley type inelastic background subtraction has been applied. Refer to the BE values assigned to the specific species (such as lattice oxygen, adsorbed oxygen, Co³⁺, and Co²⁺) in the literature as well as in the handbook, the corresponding deconvoluted peaks are added in the spectra. Note that the peak type (s, p, d, and f) should be properly selected for the specific element, and the setting for the Lorentzian-Gaussian is 20%. First, the inputted parameter estimates can be optimized separately within a proper range. Then "Optimize All" can be done optionally. As stated by the software, repeating "Optimize All" is possible provided that the resulting fitted envelope is truly improved. The fitting effectiveness is checked based on empirical judgment together with the generated $\sum\chi^2$ value which is in the range of 1.51-2.64 for the curve-fitting applied to the Co 2p_{3/2} peaks of this study. In order to verify the possible impact of spectrum smoothing on deconvolution, the same curve-fitting procedure was applied to the raw spectrum as well as the smoothed one of Au/*c*-Co₃O₄. The Co³⁺/Co²⁺ ratios obtained in

the two cases were found to be essentially identical, confirming that the employed smoothing does not affect the validity of curve-fitting results.

Catalyst activity

Catalyst of 50 mg was placed into a quartz tube reactor and evaluated in CO oxidation operated at atmospheric pressure. The feed gas (1.6% CO, 21.0% O₂, and balanced N₂) was passed through the catalyst bed at a total flow rate of 25 ml min⁻¹, giving a corresponding gas hourly space velocity (GHSV) of 30,000 ml g_{cat}⁻¹ h⁻¹. For comparison, the catalysts were first pretreated in a flow of He, or a reaction feed at 180 °C for 2 h. The feed gas mixture was directly purchased and each gas component is of high-pure grade, the moist in the feed gas mixture is < 50 ppm. The gas mixture was directly used without further dehydration. The inlet and outlet gas compositions were analyzed online using a gas chromatograph (GC-122). Both the Co₃O₄ substrates and the Au species were active for the reaction, the TOFs were thus estimated based on the total surface areas of samples rather than that of Co₃O₄ or Au individual, which were determined by physisorption of N₂ at 77 K (BET). Low CO conversion levels at a given temperature were generally used in comparison of reaction rates unless it is not applicable.

Results and discussion

XRD/ N₂ sorption measurement

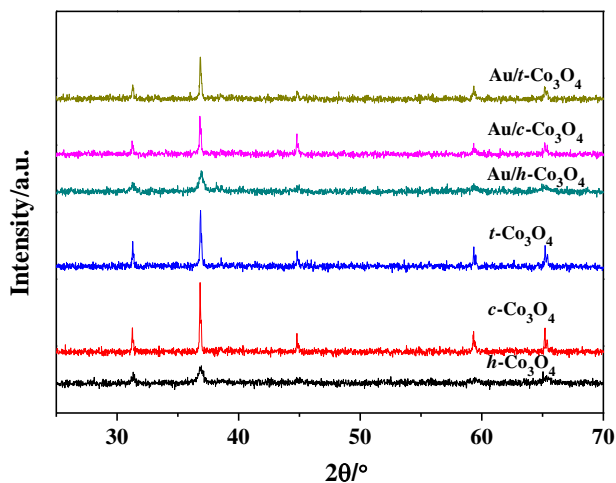


Fig. 1 XRD patterns of the Co₃O₄ polyhedrons and the Au-loaded samples.

According to the XRD patterns of different samples shown in Fig. 1, only the Co₃O₄ phase structure can be identified (JCPDS 42-1467)⁵². In our early study, we found that under the same hydrothermal conditions, the morphology of Co₃O₄ can be significantly affected by employing different amount of starting Co salt, specific oxidant (KClO₃), and especially the

morphology directing agents such as sodium citrate and PVP. In this study, the morphology of Co₃O₄ was controlled by changing the pH of preparation medium (concentration of ammonia or NaOH solution). Among the Co₃O₄ samples of different morphology, the Co₃O₄ hexagonal plates show relatively low peak intensity, indicating comparably low sample crystallinity. It is worth noting that the morphology-controlled synthesis of Co₃O₄ polyhedrons was found to be sensitive to the ambient environment especially the air to which the β-Co(OH)₂ precursor can be readily oxidized to Co³⁺ species, and the formation of Co³⁺ species is unfavorable for receiving the morphologically uniform samples. Isolating the β-Co(OH)₂ precursor from the oxidative atmosphere by a nitrogen flow passing through the flask can effectively fix the issue. In those Au-loading samples, the Co₃O₄ phase structure is essentially retained.

N₂ adsorption-desorption isotherms of *c*-Co₃O₄, *h*-Co₃O₄, *t*-Co₃O₄, and the Au-loaded samples were measured, and usually the type II (V) isotherms with inconspicuous hysteresis loops were observed (not shown). The BET surface areas of various samples are listed in Table 1. Due to the feature of single crystallites of Co₃O₄ polyhedrons under sub-micrometer scale, the specific surface areas (including those of Au-containing samples) are usually < 25 m²/g.

Table 1 BET surface areas of the Co₃O₄ and Au/Co₃O₄ samples of different morphologies

Sample	BET surface area (m ² g ⁻¹)
<i>t</i> -Co ₃ O ₄	7.5
<i>c</i> -Co ₃ O ₄	4.2
<i>h</i> -Co ₃ O ₄	20.3
Au/ <i>t</i> -Co ₃ O ₄	4.7
Au/ <i>c</i> -Co ₃ O ₄	3.1
Au/ <i>h</i> -Co ₃ O ₄	19.4

SEM/(HR)TEM

Fig. 2 illustrated the morphologically uniform *c*-Co₃O₄, *h*-Co₃O₄, and *t*-Co₃O₄ samples. *c*-Co₃O₄ showed an average edge length of ca. 400 nm, *t*-Co₃O₄ has a dimension of similar scale, while *h*-Co₃O₄ demonstrates a plate width of around 300 nm with a thickness of 30-40 nm. The HRTEM images (Figs. 2d, e) revealed that the dominant facet of *c*-Co₃O₄ and *h*-Co₃O₄ is (001) and (112), respectively^{6,36}.

In view of Fig. 2b, two types of *t*-Co₃O₄ polyhedrons can be distinguished: major *t*-Co₃O₄ I and minor *t*-Co₃O₄ II, and they are schematically illustrated in Figs. 2f & g. It is technically difficult to collect clear HRTEM images of *t*-Co₃O₄ along a certain crystal axis because of adjacent facet interference. Note that both *t*-Co₃O₄ I and *t*-Co₃O₄ II possess (001) and (111) facets.

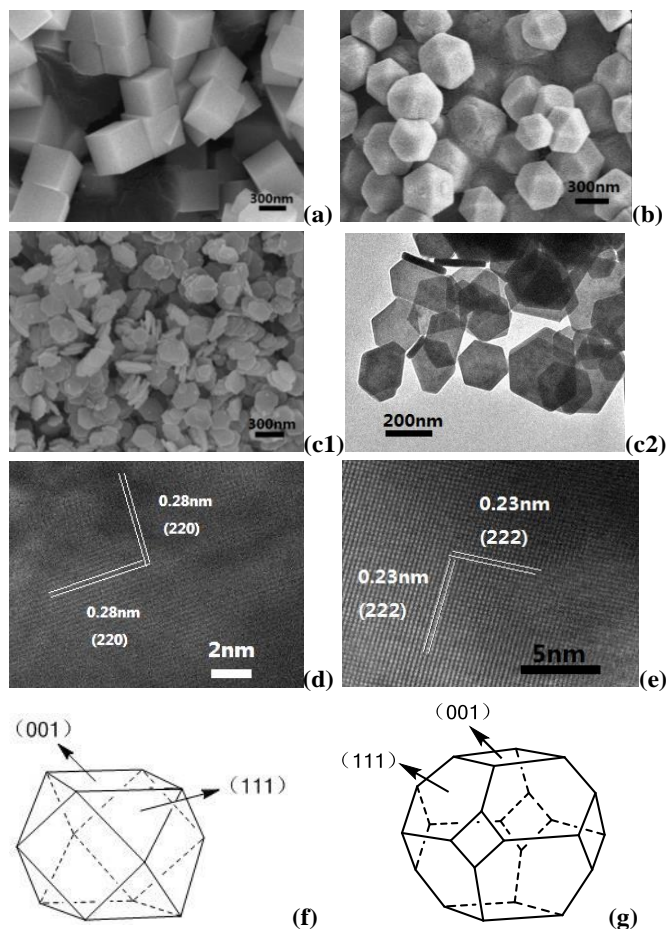


Fig. 2 SEM images of (a) *c*-Co₃O₄, (b) *t*-Co₃O₄, and (c1) *h*-Co₃O₄; TEM image of (c2) *h*-Co₃O₄; HRTEM images of (d) *c*-Co₃O₄, and (e) *h*-Co₃O₄; (f) major *t*-Co₃O₄ I, and (g) minor *t*-Co₃O₄ II.

The TEM images of the Au-loaded Co₃O₄ samples are shown in Fig. 3. With a careful deposition-precipitation process, the Au NPs were uniformly dispersed on the regularly shaped *c*-Co₃O₄, *h*-Co₃O₄, and *t*-Co₃O₄, without specific facet preferential deposition (Figs. 3a-c). Note that to control the pH of suspension by employing a diluted ammonium solution is crucial to achieve small sized yet uniform Au dispersion. The free NH₃ molecules may function as the ligands to stabilize the Au³⁺ cations in the synthetic medium meanwhile a low concentration of generated OH⁻ can mildly increase the pH value of synthetic medium to around 9. The statistical analysis of the Au particle size of three Au loaded samples (Fig. 4) indicated that the Au particle size is rather close to each other: 3.3 ± 1.2 nm on Au/*c*-Co₃O₄, 3.1 ± 0.9 nm on Au/*h*-Co₃O₄, and 3.3 ± 1.0 nm on Au/*t*-Co₃O₄. In order to investigate the Au particle size effect, smaller Au NPs were deposited on *h*-Co₃O₄ with the particle size distribution of 1.6 ± 0.6 nm (Fig. S1). There might be a concern that the deposition of Au NPs could disturb the structure of the Co₃O₄ surface. A detailed investigation on the deposition of Au clusters of different size

(1-5 nm) on TiO₂ (110) by means of STM was reported by Goodman and coworkers⁵³, and the results indicated that the disturbing of substrate surface by Au clusters is insignificant. In this study, the Au/Co₃O₄ (001) and Au/Co₃O₄ (112) interfaces were also studied by means of HRTEM and the results (Figs. 3d and e) indicated that perturbing of Co₃O₄ substrate surfaces is also insignificant.

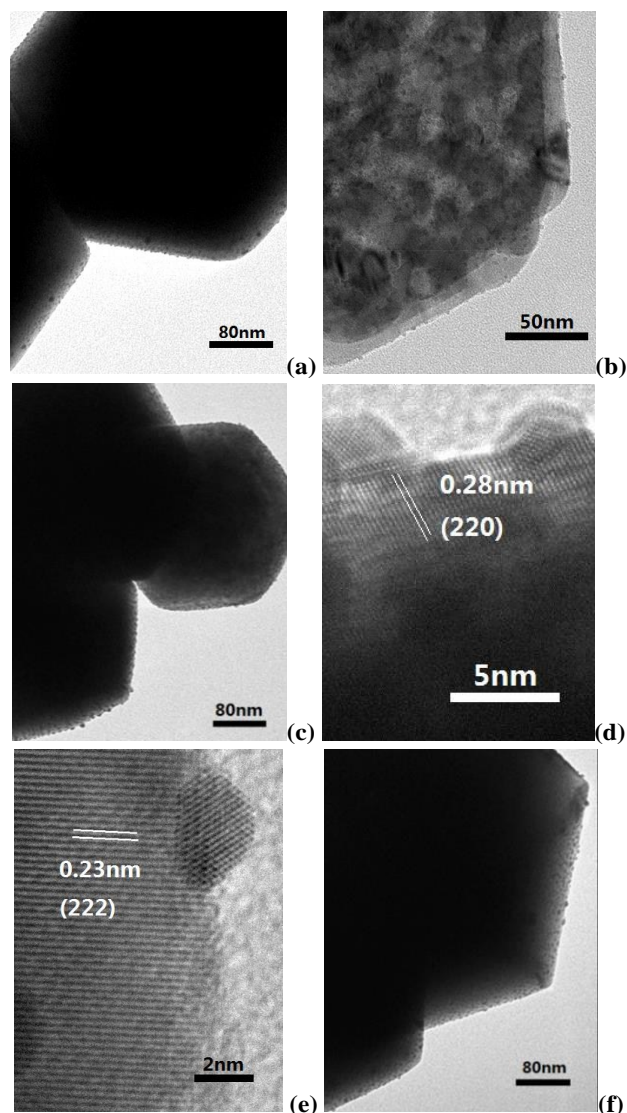


Fig. 3 TEM images of (a) Au/*c*-Co₃O₄, (b) Au/*h*-Co₃O₄, and (c) Au/*t*-Co₃O₄; HRTEM images of (d) Au/*c*-Co₃O₄, and (e) Au/*h*-Co₃O₄; TEM image of (f) used Au/*c*-Co₃O₄.

In this study, the Au/Co₃O₄ interface is considered as a whole; and since the structure deviation of Co₃O₄ substrate surface upon Au deposition is insignificant, the comparison made between different interfaces is reasonable. Au NPs could aggregate when they were experienced calcination and/or reaction, and this may adversely influence the application of Au NPs when the operation and regeneration of catalysts at

elevated temperature are needed⁵⁴. The Au dispersion and the morphology of Co_3O_4 substrates before and after reaction have been checked, they are essentially preserved as shown in Fig. 3f and Fig. S2.

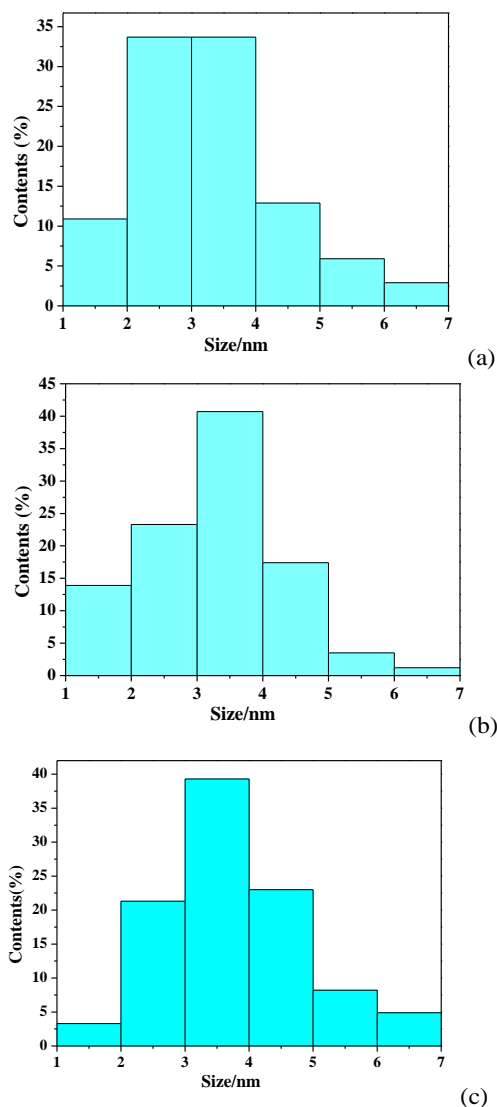


Fig. 4 Au particle size distribution of (a) Au/c- Co_3O_4 (3.3 ± 1.2 nm), (b) Au/h- Co_3O_4 (3.1 ± 1.0 nm), and (c) Au/t- Co_3O_4 (3.3 ± 1.0 nm).

H₂-TPR

H₂-TPR profiles of *c*- Co_3O_4 , *h*- Co_3O_4 , *t*- Co_3O_4 , and the Au-loaded samples are shown in Fig. 5. Among three Co_3O_4 polyhedrons, *h*- Co_3O_4 shows the presence of more reactive lattice oxygen species—characterized by a small peak centred around 320°C. The reduction of *c*- Co_3O_4 and *t*- Co_3O_4 looks not so different as in the case of *h*- Co_3O_4 . However, if one compares the reduction profiles of *c*- Co_3O_4 and *t*- Co_3O_4 in the low temperature region where the reduction of surface adsorbed/lattice oxygen occurs (Fig. S3), clearly that of *c*-

Co_3O_4 is more reactive. The dominant facet of *h*- Co_3O_4 is (112), while that of *c*- Co_3O_4 is (001) and that of *t*- Co_3O_4 are (001) and (111). Therefore, one can estimate the reactivity of surface oxygen on three facets is (112) > (001) > (111). The more reducible surface oxygen atoms are associated with an open surface structure of (112) facet on which a lower density of surface oxygen is presented. Au addition notably enhanced the reduction of surface oxygen, particularly in the case of Au/h- Co_3O_4 , suggesting that the Au/(112) interface is the most reactive with respect to its surface oxygen species.

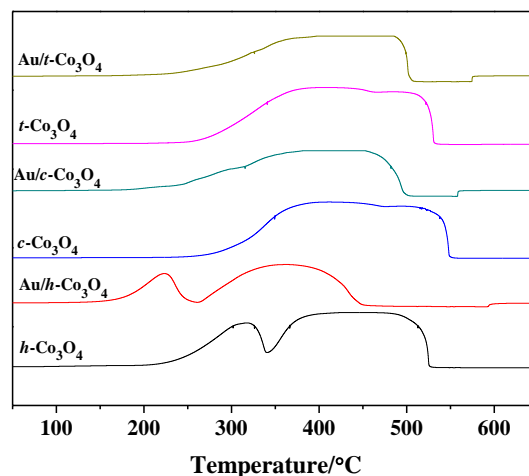


Fig. 5 H₂-TPR profiles of the Co_3O_4 polyhedrons (*c*- Co_3O_4 , *h*- Co_3O_4 , and *t*- Co_3O_4) and the related Au-loaded samples.

XPS

The results of XPS investigation on the selected samples (without and with pretreatment) are shown in Fig. 6. The binding energies (BEs) of Au 4f_{7/2} as well as Au 4f_{5/2} of the untreated Au/h- Co_3O_4 are 84.0 and 87.6 eV, respectively; while that of the untreated Au/c- Co_3O_4 are 83.8 eV and 87.5 eV, respectively (Fig. 6a). The observation suggested that although the Au NPs are essentially in metallic state, those on the *h*- Co_3O_4 could be slightly electron deficient as compared with the ones on the *c*- Co_3O_4 ⁵⁵. As for the He-treated Au/c- Co_3O_4 , the BEs of Au 4f_{7/2} and Au 4f_{5/2} are 83.9 and 87.6 eV, respectively. Clearly, the pretreatment in He-atmosphere showed minor impact on the oxidation state of Au NPs. It is worth mentioning that if a comparison is made between the two “isolated” samples, a difference of 0.2 eV in the BE of Au4f could be too small, and the conclusion will be ambiguous. In this study, since the same measurement is conducted on the Au NPs of almost same size deposited over the certain facets of Co_3O_4 substrate, the situation is thought to be relatively simple. The observed small difference in the BE of Au component could be a result of the specific Au- Co_3O_4 interfacial contact. Note that an overall electron property of Au cluster on *h*- Co_3O_4 and *c*- Co_3O_4 does not differ appreciably.

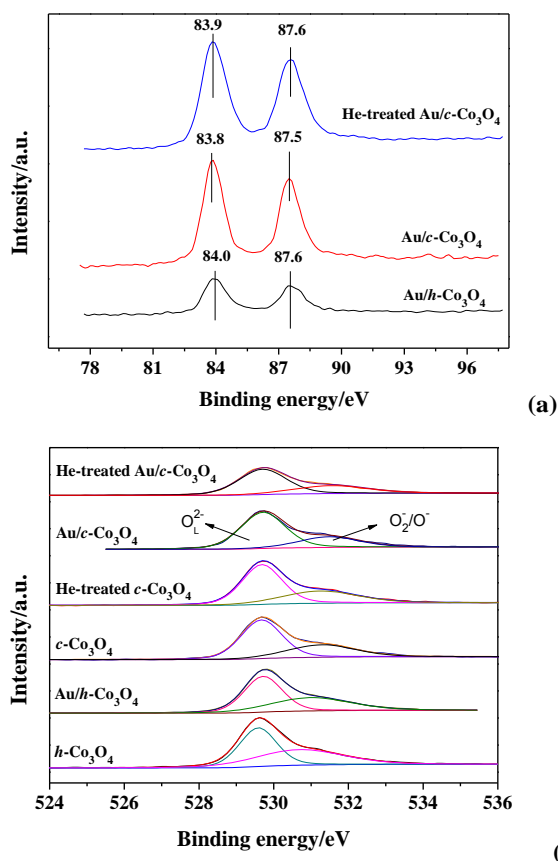


Fig. 6 (a) Au 4f XPS spectra of (a) the untreated Au/c-Co₃O₄ and Au/h-Co₃O₄ as well as He-treated Au/c-Co₃O₄, and (b) O 1s XPS spectra of the untreated *h*-Co₃O₄, Au/h-Co₃O₄, and Au/c-Co₃O₄ together with He-treated *c*-Co₃O₄ and Au/c-Co₃O₄.

The O1s XPS spectra of the untreated *c*-Co₃O₄ and *h*-Co₃O₄, Au/c-Co₃O₄, and Au/h-Co₃O₄ together with the treated Au/c-Co₃O₄ and Au/h-Co₃O₄ are shown in Fig. 6b. The peak with binding energy at ca. 529.7 eV is related to the lattice oxygen (O_L²⁻), whereas the peaks at 530.7-531.6 eV is associated with surface oxygen adspecies. Quite a few studies^{47, 48, 56a-e, 57} suggested that there are nucleophilic (lattice oxygen) and electrophilic (adsorbed oxygen such as O₂⁻ and O⁻) species assigned in terms of the low (528-531 eV) and high BEs (> 531 eV). Bear in mind that these serve as guidelines rather than as strict rules for assigning spectra. In Fig. 6, all of the O1s peaks nearly end at 533 eV, suggesting that the OH and particularly the surface carbonate species should be quite limited in amount. Therefore, the curve-fitting does not include these two components. The fitting results can reflect a tendency of different oxygen species changing with Au deposition and/or pretreatment, and the tendency is also found to be coincident with the observed catalytic behaviors. It was observed that the BEs of lattice oxygen is little affected by Au deposition and/or pretreatment. However, the BEs and amount of O₂⁻/O⁻ varied notably up Au deposition and/or pretreatment. For instance, Au deposition on *h*-Co₃O₄ somewhat decreases the fraction of

O₂⁻/O⁻ meanwhile causes the peak shift associated with O₂⁻/O⁻ (from 530.7 to 531.1 eV). Note that a similar trend was observed over *c*-Co₃O₄ and Au/c-Co₃O₄. Compare the spectra of *c*-Co₃O₄ and He-treated one, one can find that there seems an insignificant change with respect to the O_L²⁻ as well as O₂⁻/O⁻ species after pretreatment.

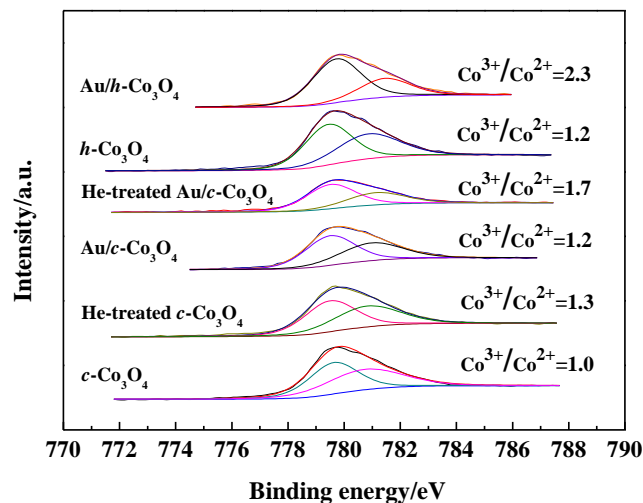


Fig. 7 Deconvolution analyses of the Co 2p_{3/2} XPS peaks of *c*-Co₃O₄, He-treated *c*-Co₃O₄, Au/c-Co₃O₄, He-treated and Au/c-Co₃O₄, *h*-Co₃O₄, and Au/h-Co₃O₄.

The same pretreatment of Au/c-Co₃O₄ results in an obvious change associated with the O₂⁻/O⁻, namely, a noticeable reduction in the fraction of O₂⁻/O⁻ meanwhile the peak shift from 531.5 to 531.6 eV. Decrease in peak intensity in the range of 530.7-531.6 eV implies a less density of O₂⁻/O⁻ while the peak shift toward higher BE end corresponds a higher fraction of O⁻ in the total of O₂⁻/O⁻ species. Based on these observations, one can infer that Au deposition on *c*-Co₃O₄ reduced the overall amount of O₂⁻/O⁻, particularly that of O₂⁻. Au deposition on *h*-Co₃O₄ caused the most significant reduction in O₂⁻/O⁻. This is understandable, because the *h*-Co₃O₄ has the dominant (112) facet which is more structurally open, and more structural defects (such as oxygen vacant sites) can present on the surface of *h*-Co₃O₄ where more O₂⁻/O⁻ species could form. With Au nucleation, some of the structural defects can be eliminated, and less O₂⁻/O⁻ species formed. The density of O₂⁻/O⁻ (particularly the former) on the Au entities should not be high. Pretreatment on *c*-Co₃O₄ showed minor effect on the O₂⁻/O⁻ species, while pretreatment on Au/c-Co₃O₄ noticeably reduced the fraction of the O₂⁻/O⁻ species (particularly the former). The change of O₂⁻/O⁻ amount with Au deposition and/or pretreatment is thought to be important to show effect on the catalytic activity^{46,47,57,58}.

As for the oxidation state of the Co species, note that the Co2p spectra of different cobalt compounds may exhibit sometime satellite structure. And this may also complicate the assignment and quantification of Co²⁺ and Co³⁺ species. In the

present case, the cobalt substrate is the same type (Co_3O_4), and the spectra of samples are recorded under the identical conditions and analyzed on the same basis. The fitting is based on the $\text{Co } 2\text{P}_{3/2}$ peak with subtraction of satellite background. The $\text{Co}^{3+}/\text{Co}^{2+}$ ratios are thus estimated for a parallel comparison. A tendency of $\text{Co}^{3+}/\text{Co}^{2+}$ ratios is interpreted in line with Au deposition and pretreatment. One can see that Au deposition onto *h*- Co_3O_4 noticeably increased the surface Co^{3+} fraction ($\text{Co}^{3+}/\text{Co}^{2+}$ ratio varying from 1.2 to 2.3, Fig. 7); while Au deposition on *c*- Co_3O_4 slightly increased the surface $\text{Co}^{3+}/\text{Co}^{2+}$ ratio (from 1.0 to 1.2). Note also that the He-pretreatment on *c*- Co_3O_4 also enhanced the surface $\text{Co}^{3+}/\text{Co}^{2+}$ ratio (from 1.0 to 1.3), while the He-pretreatment on Au/*c*- Co_3O_4 would notably increase surface $\text{Co}^{3+}/\text{Co}^{2+}$ ratio (from 1.2 to 1.7). An obvious increment in surface $\text{Co}^{3+}/\text{Co}^{2+}$ ratio (from 1.3 to 1.7) was also observed between the treated *c*- Co_3O_4 and Au/*c*- Co_3O_4 . The variations in the surface $\text{Co}^{3+}/\text{Co}^{2+}$ ratio would show a great impact on catalytic activity^{11,36}, which will be discussed in the next section.

Structural models

To better understand the surface properties of the Co_3O_4 substrates and the Au- Co_3O_4 interfaces, a close view of the structural arrangements of the (001), (111), and (112) facets of Co_3O_4 and those of Au- Co_3O_4 interfaces are illustrated in Fig. 8. In light of Figs. 8a and b, there are lower density of Co^{2+} ions while higher density of Co^{3+} as well as lattice oxygen (O_L^{2-}) on the exposed (001) facet. The opposite situation can be observed on the exposed (111) facet. Although the O1s spectra of *c*- Co_3O_4 changed insignificantly upon He-pretreatment, the surface $\text{Co}^{3+}/\text{Co}^{2+}$ ratio was observed to increase noticeably. Since the XPS technique is not topmost layer-limited and the total amount of lattice oxygen in the detectable surface region is greater than that of $\text{Co}^{3+}/\text{Co}^{2+}$ ions, it is understandable the ratio of surface $\text{Co}^{3+}/\text{Co}^{2+}$ is more sensitive to the pretreatment. As a matter of fact, an increment in surface $\text{Co}^{3+}/\text{Co}^{2+}$ ratio may imply the removal of O_2^-/O^- to certain extent.

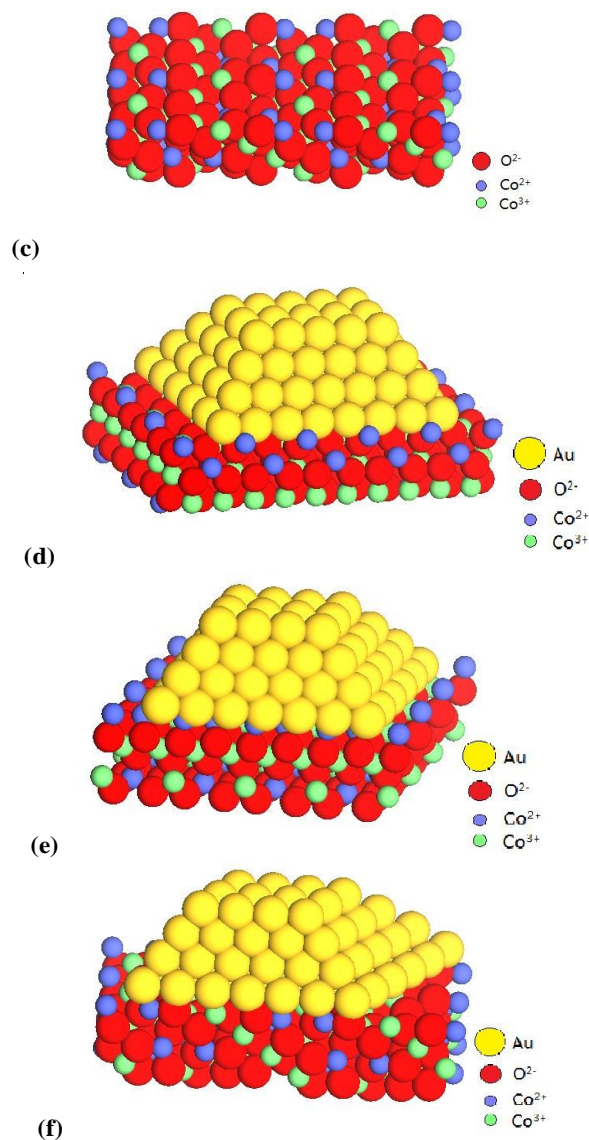
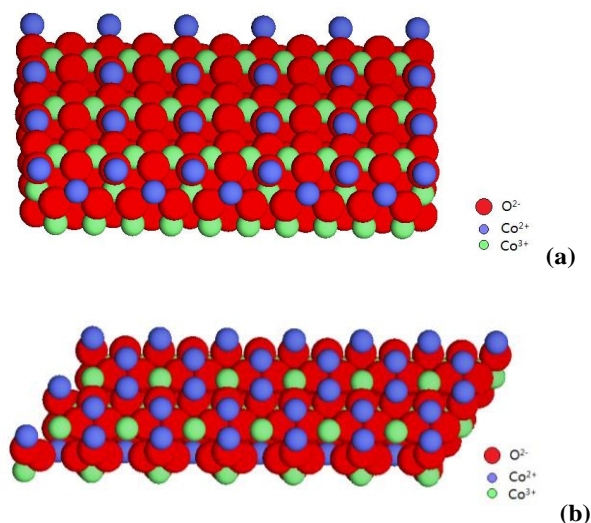


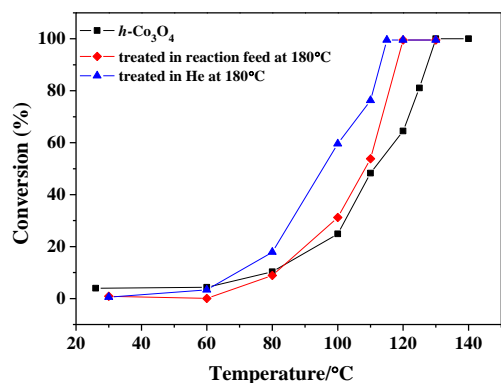
Fig. 8 Schematic illustrations of (a) (001), (b) (111), and (112) facets of Co_3O_4 substrates; (d) Au/ Co_3O_4 (001), (e) Au/ Co_3O_4 (111), and Au/ Co_3O_4 (112) interfaces.

The creation of surface vacant sites by pretreatments of Co_3O_4 at moderate temperature was early suggested by Haruta and his co-workers⁴⁵. Based on the structural arrangements of the (001), (111), and (112) facets of Co_3O_4 substrates, one can infer that the deposited Au atoms on the (111)/(112) facets are comparably electron deficient because they can more closely contact with the exposed $\text{Co}^{3+}/\text{Co}^{2+}$ ions, and this is coincident with the experimental observation. Deposition of Au NPs on the (001), (111), and (112) facets of Co_3O_4 substrates can also somewhat modify the surface $\text{Co}^{3+}/\text{Co}^{2+}$ ratio, because on each facet the covered Co^{3+} and Co^{2+} fraction by the deposited Au clusters is different. In view of the structural models for different Co_3O_4 facets as well as the Au- Co_3O_4 interfaces, one can reasonably infer that when the Au dispersion is comparable,

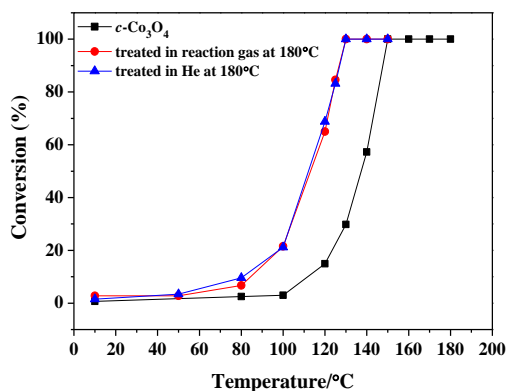
there are more surface oxygen atoms associated with the Au- Co_3O_4 boundary on the Au/(001) Co_3O_4 because of a higher exposure of surface lattice oxygen on the (001) facet of Co_3O_4 . Similar situation is likely happened on the Au/(112) interface. Such kind of surface oxygen atoms is thought to be more reactive (effectively weakened due to the Au- Co_3O_4 interaction) and can migrate along the surface to form the O_2^-/O^- species, or can be eliminated upon pretreatment to leave the surface oxygen vacant sites around the Au- Co_3O_4 boundary. These presumptions are experimentally evidenced by the XPS investigation (Fig. 6b). Duan and Henkelman recently suggested the importance of the Au/ TiO_2 boundary (particularly the Au/ Ti_{5c} Site) for CO oxidation⁵⁹. Bear in mind that the comparisons should be made on the certain prerequisites: the Co_3O_4 substrates are well shaped and have certain plane orientations, meanwhile the size and dispersion of Au NPs are also comparable.

Catalytic activity

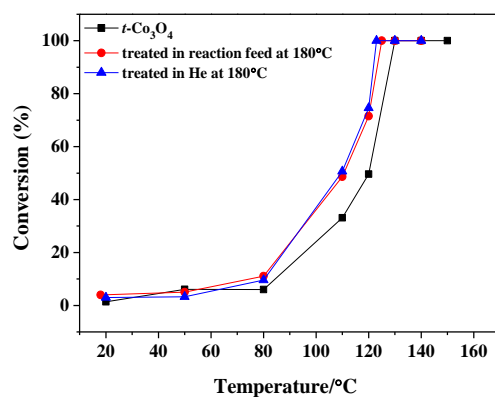
Low temperature CO oxidation on *c*- Co_3O_4 , *h*- Co_3O_4 , and *t*- Co_3O_4 as well as on the Au-loaded samples was systematically studied and compared. All of the samples were tested as synthesized (without pretreatment), treated in an inert atmosphere of He at 180°C for 2 h, and treated in a reaction atmosphere of $\text{CO}/\text{O}_2/\text{N}_2$ ($v/v/v=1.6/21.0/77.4$) at 180°C for 2 h.



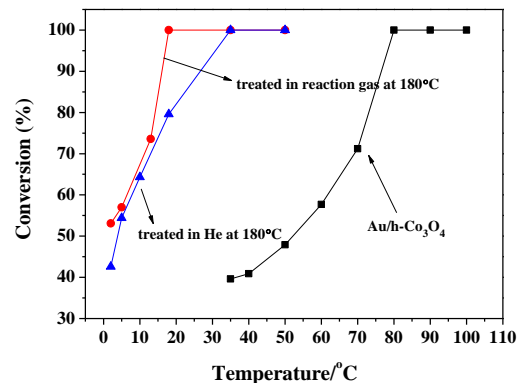
(a)



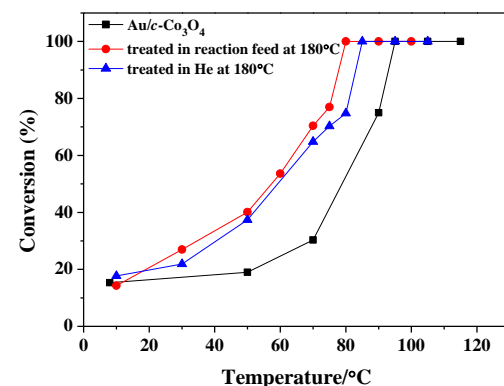
(b)



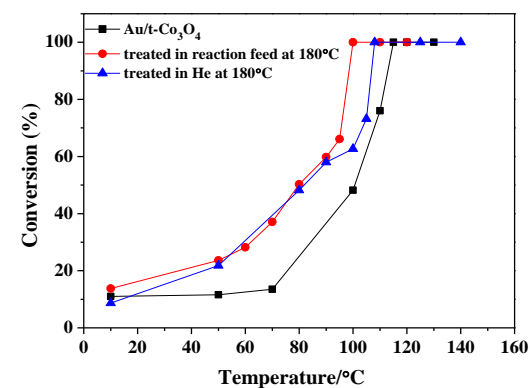
(c)



(d)



(e)



(f)

Fig. 9 Temperature dependence of CO conversions over various catalysts without and with He- and in situ-pretreatments.

For the three Co₃O₄ polyhedrons without Au NPs deposition, the pretreatment showed different effect: obvious enhancement in activity was observed on both *c*-Co₃O₄ and *h*-Co₃O₄, while only slight enhancement on *t*-Co₃O₄. Except for *h*-Co₃O₄ on which pretreating sample in an inert atmosphere seemed more favorable for reaction, both *c*-Co₃O₄ and *t*-Co₃O₄ showed almost identical effect on activity upon the pretreatment in either an inert atmosphere or a reaction feed. The results demonstrated that although three facets of Co₃O₄ substrate are sensitive to the pretreatment for CO oxidation; the (112) and (001) ones behave more evidently (Figs. 9a, b vs c). The reaction rates normalized to per surface area of sample clearly supported this conclusion (Table 2).

Over the Co₃O₄ polyhedrons, the most significant enhanced activity was observed on the pre-treated *c*-Co₃O₄ (increment to approximately 370% based on the He-treated TOF value, the same below), a modest enhancement in activity was obtained on the pre-treated *h*-Co₃O₄ (increment to approximately 210%), while the smallest enhancement in activity was observed on the pre-treated *t*-Co₃O₄ (increment to approximately 160%). The same order can be obtained when a comparison was made among the ΔT_{50} values.

Table 2 Activities comparison over the Co₃O₄ polyhedrons and the Au-loaded samples without and with the pretreatments

Sample	Pretreatment	Temp. (°C)/ Conv. (%)	T_{50} (°C)	TOF ^a ($\mu\text{mol m}^{-2} \text{min}^{-1}$)
<i>t</i> -Co ₃ O ₄	Non	80/6.0	120	0.14
	He	80/9.6	110	0.23
	Reaction feed	80/11.1	113	0.26
<i>c</i> -Co ₃ O ₄	Non	80/2.5	138	0.11
	He	80/9.6	112	0.41
	Reaction feed	80/6.7	114	0.28
<i>h</i> -Co ₃ O ₄	Non	80/10.3	112	0.09
	He	80/21.7	95	0.19
	Reaction feed	80/13.1	109	0.12
Au/ <i>t</i> - Co ₃ O ₄	Non	50/11.6	100	0.44
	He	50/21.8	81	0.83
	Reaction feed	50/23.6	80	0.90
Au/ <i>c</i> - Co ₃ O ₄	Non	50/19.0	80	0.79
	He	50/37.4	60	2.16
	Reaction feed	50/40.1	58	2.32
Au/ <i>h</i> - Co ₃ O ₄	Non	35/39.6	55	0.36
	He	2/42.6	4	0.39
	Reaction feed	2/53.1	< 2	0.49

^a For the Co₃O₄ polyhedrons, the CO conversions at 80°C (the conversion level is in the range of 6-21.7%) were used to calculate the TOFs; while for the Au-loaded samples, except for Au/*h*-Co₃O₄, the CO conversions at 50°C (the conversion level is in the range of 11.6-40.1%) were used to calculate the TOFs. For Au/*h*-Co₃O₄, the reaction temperature needs to be decreased to 35°C (without pretreatment) and 2°C (with pretreatment) to control the CO conversion level. The TOF values are calculated on the basis of specific surface area of sample.

With Au NPs deposition on three Co₃O₄ polyhedrons, the CO oxidation activity was significantly increased regardless of pretreatment or not. Among the Au/Co₃O₄ without pretreatments, the Au/*h*-Co₃O₄ exhibited the highest activity (Fig. 9d, $T_{50} = 55^\circ\text{C}$), meanwhile Au/*c*-Co₃O₄ and Au/*t*-Co₃O₄ also showed notable increase in activity (Fig. 9d, $T_{50} = 80$ and 100°C respectively). When comparing Au/*c*-Co₃O₄ and Au/*t*-Co₃O₄, one would find the (001) facet is the major one existing on *c*-Co₃O₄ and *t*-Co₃O₄, while the (111) facet only exists on *t*-Co₃O₄. However, the resulting enhancement in activity by Au deposition is actually more evident on Au/*c*-Co₃O₄ other than Au/*t*-Co₃O₄. The observations suggested that the Au/(001) interface appears inherently more active than the Au/(111) one for CO oxidation.

For Au/*h*-Co₃O₄, the excellent activity on the basis of per unit mass of catalyst should originate from several factors. This sample has the largest specific surface area (Table 1). The XPS study revealed that the surface Co³⁺/Co²⁺ ratio increased the most significantly upon Au NPs deposition; meanwhile the deposited Au NPs are also slightly electron deficient, which favored CO adsorption. A lower density of oxygen adspecies on the Au NPs⁵⁸ plus a higher fraction of surface Co³⁺ are thought to be favorable for CO oxidation^{46,60-64}. Actually we also found an Au particle size effect on CO oxidation activity for Au/*h*-Co₃O₄. As the Au NPs decrease in size to 1.6 nm, the activity can be further increased (Fig. S4), although the Au NPs smaller than 2 nm were considered to be less strength in metallic nature^{65,66}. However, the enhancement in activity by He-pretreatment seems to be insignificant over s-Au/*h*-Co₃O₄ (1.6 ± 0.6 nm).

Upon a pre-treatment in He or reaction feed, additional enhancement in activity was observed over the Au-Co₃O₄ interfaces, and the extent of enhancement is certainly Au-Co₃O₄ interface dependent. Based on the TOF values listed in Table 2, an increment to approximately 270% in activity was achieved on Au/*c*-Co₃O₄; while an increment to approximately 190% was observed over Au/*t*-Co₃O₄. It is difficult to compare the activity of Au/*h*-Co₃O₄ before and after pretreatment based on the TOF values, because it is impossible to select a certain temperature at which the CO conversion level is applicable. Nevertheless, in terms of the ΔT_{50} values, one can conclude that the activity enhancement upon pretreatment is the most significant over Au/*h*-Co₃O₄. Clearly, there is an order in activity enhancement upon pretreatment among the three Au-Co₃O₄ interfacial structures: Au/(112) > Au/(001) > Au/(111).

Xie et al.¹¹ found that the unique exposed crystal facet of Co₃O₄ nanorods can be extremely active for CO oxidation. Teng et al.⁴⁰ also demonstrated the facet-dependent activity on the Co₃O₄ nanocrystals in CO oxidation. The results of current study extended the insights into the interface-dependent activity over the well-controllably prepared Au-Co₃O₄ interfacial structures. Liu et al.⁶⁷ synthesized the ordered mesoporous Co₃O₄ supported Au catalysts for CO and VOCs combustion. The mesoporous Co₃O₄ supported Au NPs seemed to be more active than the Au/Co₃O₄ polyhedrons of this study for CO oxidation, although the Au particle size distribution is similar in the two studies. The method used for Au introduction, however,

was rather different: in the present case, the Au introduction was achieved via a DP process, while in the case of Au/mesoporous Co_3O_4 , the Au introduction was established via chemical reduction of HAuCl_4 with NaBH_4 and adsorption of Au colloid particles. Therefore, the nature of Co_3O_4 substrate as well as the Au NPs and the involved Au- Co_3O_4 interaction could be greatly influenced by preparation history, which in turn accounted for the difference in activity of these Au/ Co_3O_4 systems. Li et al.⁶⁸ reported CO oxidation over the iodine-ion-induced size-tunable Co_3O_4 nanowires. The catalyst was highly efficient by employing extraordinarily high value of GHSV, but it became almost inactive below 100 °C and deactivated with TOS below 120°C. Bear in mind that catalyst performance is also rather sensitive to reaction conditions applied. For examples, the catalytic activity can change remarkably due to different content of moisture in the reaction feed gas⁴⁶, while the very reactive Au catalysts also suffered poor catalyst durability especially when a high content of moisture was presented^{37,69}. Cautions should be taken to make comparisons among the results reported.

We further investigated catalyst reliability and durability on the three representative *s*-Au/*h*- Co_3O_4 , Au/*h*- Co_3O_4 , and Au/*t*- Co_3O_4 catalysts, and the results are supplemented in Figs. S5, 6. Concerning catalyst reliability, each sample has tested twice, and the activities obtained in the first and second running are compared. Fig. S5 indicates that the catalysts show acceptable repeatability in activity. As for catalyst durability, each sample has been operated for a period of 30-50 h. *s*-Au/*h*- Co_3O_4 is rather durable with time on stream up to 50 h (Fig. S6a). Au/*h*- Co_3O_4 decreases in activity to some extent in the first 5 h and then almost retains the activity afterwards (Fig. S6b). Au/*t*- Co_3O_4 slightly decreases in activity with time on stream of 25-28 h (Fig. S6c). Note that, on both Au/*h*- Co_3O_4 and Au/*t*- Co_3O_4 , durability test was directly performed after activity repeatability test; therefore, the mentioned activity drop on Au/*h*- Co_3O_4 and Au/*t*- Co_3O_4 actually corresponds to an overall time on stream of ca. 25 and 45 h, respectively.

Conclusions

In the current study, careful synthesis of the morphologically uniform *c*- Co_3O_4 , *h*- Co_3O_4 and *t*- Co_3O_4 was accomplished; and the crystalline orientations, namely, the (001), (111), and (112) facets of these Co_3O_4 polyhedrons were identified. Precise Au NPs deposition with a well-controlled particle size distribution (3.1-3.3 nm) was achieved on the Co_3O_4 entities to gain the exclusive Au- Co_3O_4 interfaces which allow us to make a detailed comparison on the basis of their unique interface structures and eventually their catalytic behaviors. The H_2 -TPR and XPS investigations revealed the important deviations in reactivity of surface oxygen, surface $\text{Co}^{3+}/\text{Co}^{2+}$ ratio, evolution of surface oxygen species/vacant sites, as well as the Au oxidation state upon Au loading and specific pretreatments. The enhanced CO oxidation by Au deposition and particularly He- and in situ-pretreatments are clarified in light of their structural specialties, and the following order for Co_3O_4 substrate and Au-

Co_3O_4 interface is derived: (001) > (112) > (111), and Au/(112) > Au/(001) > Au/(111). The results of Au/*h*- Co_3O_4 also suggest that both Au entity and structural feature of Co_3O_4 can affect on the catalytic behavior of generated interface. The current study extended the insights into the interface-dependent CO oxidation over the controllably prepared Au- Co_3O_4 interfacial structures.

Acknowledgements

We greatly appreciated the financial support from NSFC (21173118, 21373110), MSTC (2013AA031703), and MOE (20110091110023).

Notes and references

^a Key Laboratory of Mesoscopic Chemistry, MOE, School of Chemistry and Chemical Engineering, Nanjing University, 22 Hankou Road, Nanjing 210093, China. Fax: +86-25-83317761; Tel: +86-25-83686270; E-mail: jiwj@nju.edu.cn.

^b Department of Chemistry, Hong Kong Baptist University, Hong Kong, China, Fax: +852-34117348; E-mail: pctau@hkbu.edu.hk

† Electronic supplementary information (ESI) available: TEM image and Au particle size distribution of *s*-Au/*h*- Co_3O_4 (1.6 ± 0.6 nm); TEM image of used Au/*h*- Co_3O_4 and Au particle size distribution of used Au/*c*- Co_3O_4 and Au/*h*- Co_3O_4 (3.5 ± 0.8 nm) and (c) Au particle size distribution of used Au/*c*- Co_3O_4 (3.9 ± 1.2 nm); H_2 -TPR profiles of *c*- Co_3O_4 and *t*- Co_3O_4 in the 80-220°C range; Temperature dependence of CO conversions over *s*-Au/*h*- Co_3O_4 (1.6 ± 0.6 nm) without and with He-pretreatment; Activities over *s*-Au/*h*- Co_3O_4 (1.6 ± 0.6 nm) without and with He-pretreatment; Activity repeatability tests over in-situ pretreated *s*-Au/*h*- Co_3O_4 , Au/*h*- Co_3O_4 , and (c) Au/*t*- Co_3O_4 ; Catalyst durability tests over *s*-Au/*h*- Co_3O_4 , Au/*h*- Co_3O_4 , and Au/*t*- Co_3O_4 .

- 1 C. Burda, X. B. Chen, R. Narayanan and M. A. El-Sayed, *Chem. Rev.*, 2005, **105**, 1025-1102.
- 2 K. B. Zhou, X. Wang, X. M. Sun, Q. Peng and Y. D. Li, *J. Catal.*, 2005, **229**, 206-121.
- 3 Y. W. Zhang, M. E. Grass, S. E. Habas, F. Tao, T. F. Zhang, Y. R. Borodko, P. D. Yang and G. A. Somorjai, Abstracts of Papers, 234th ACS National Meeting, Boston, MA, United States, August 19-23, American Chemical Society: Washington DC, 2007, INOR-138.
- 4 N. Tian, Z. Y. Zhou, S. G. Sun, Y. Ding and Z. L. Wang, *Science*, 2007, **316**, 732-735.
- 5 R. Si and M. Flytzani-Stephanopoulos, *Angew. Chem. Int. Ed.*, 2008, **47**, 2884-2887.
- 6 L. H. Hu, Q. Peng and Y. D. Li, *J. Am. Chem. Soc.*, 2008, **130**, 16136-16137.
- 7 a) J. A. Anderson and M. F. Garcia (Eds.), Supported Metals in Catalysts, *Catalytic Science Series Vol. 5*, Imperial College Press, London, 2005; b) A. Taketoshi and M. Haruta, *Chem. Lett.*, 2014, **43**, 380-387.
- 8 Y. W. Jun, J. S. Choi and J. Cheon, *Angew. Chem. Int. Ed.*, 2006, **45**, 3414-3439.
- 9 S. E. Habas, H. Lee, V. Radmilovic, G. A. Somorjai and P. D. Yang, *Nature Mater.*, 2007, **6**, 692-697.
- 10 H. G. Yang, C. H. Sun, S. Z. Qiao, J. Zou, G. Liu, S. C. Simth, H. M. Cheng and G. Q. Lu, *Nature*, 2008, **453**, 638-642.

- 11 X. Xie, Y. Li, Z. Q. Liu, M. Haruta and W. J. Shen, *Nature*, 2009, **458**, 746-749.
- 12 J. Z. Yin, Z. N. Yu, F. Gao, J. J. Wang, H. Pang and Q. Y. Lu, *Angew. Chem. Int. Ed.*, 2010, **49**, 6328-6332.
- 13 N. Ta, J. Y. Liu, S. Chenna, P. A. Crozier, Y. Li, A. Chen and W. J. Shen, *J. Am. Chem. Soc.*, 2012, **134**, 20585-20588.
- 14 M. C. Kung, R. J. Davis and H. H. Kung, *J. Phys. Chem. C*, 2007, **111**, 11767-11775.
- 15 B. K. Min and C. M. Friend, *Chem. Rev.*, 2007, **107**, 2709-2724.
- 16 N. Lopez, T. V. W. Janssens, B. S. Clausen, Y. Xu, M. Mavrikakis, T. Bligaard and J. K. Nørskov, *J. Catal.*, 2004, **223**, 232-235.
- 17 G. J. Hutchings, M. S. Hall, A. F. Carley, P. Landon, B. E. Solsona, C. J. Kiely, A. Herzing, M. Makkee, J. A. Moulijn, A. Overweg, J. C. Fierro-Gonzalez, J. Guzman and B. C. Gates, *J. Catal.*, 2006, **242**, 71-81.
- 18 J. T. Miller, A. J. Kropf, Y. Zha, J. R. Regalbutto, L. Delannoy, C. Louis, E. Bus and J. A. van Bokhoven, *J. Catal.*, 2006, **240**, 222-234.
- 19 A. A. Herzing, C. J. Kiely, A. F. Carley, P. Landon and G. J. Hutchings, *Science*, 2008, **321**, 1331-1335.
- 20 M. Chen and D. Goodman, *Science*, 2004, **306**, 252-255.
- 21 M. Haruta, S. Tsubota, T. Kobayashi, H. Kageyama, M. J. Genet and B. Delmon, *J. Catal.*, 1993, **144**, 175-192.
- 22 X. Nie, H. Qian, Q. Ge, H. Xu and R. Jin, *ACS Nano*, 2012, **6**, 6014-6022.
- 23 H. Kung, M. Kung and C. Costello, *J. Catal.*, 2003, **216**, 425-432.
- 24 Y. Y. Wu, N. A. Mashayekhi and H. H. Kung, *Catal. Sci. Technol.*, 2013, **3**, 2881-2891.
- 25 A. F. Carley, D. J. Morgan, N. Song, M. W. Roberts, S. H. Taylor, J. K. Bartley, D. J. Willock, K. L. Howard and G. J. Hutchings, *Phys. Chem. Chem. Phys.*, 2011, **13**, 2528-2538.
- 26 M. Kotobuki, R. Leppelt, D. A. Hansgen, D. Widmann and R. J. Behm, *J. Catal.*, 2009, **264**, 67-76.
- 27 M. Haruta, *Faraday Discuss.*, 2011, **152**, 11-32.
- 28 P. Poizot, S. Laruelle, S. Grugeon, L. Dupont and J. M. Tarascon, *Nature*, 2000, **407**, 496-499.
- 29 K. T. Nam, D. W. Kim, P. J. Yoo, C. Y. Chiang, N. Meethong, P. T. Hammond, Y. M. Chiang and A. M. Belcher, *Science*, 2006, **312**, 885-888.
- 30 X. W. Lou, D. Deng, J. Y. Lee, J. Feng and L. A. Archer, *Adv. Mater.*, 2008, **20**, 258-262.
- 31 A. M. Cao, J. S. Hu, H. P. Liang, W. G. Song, L. J. Wan, X. L. He, X. G. Gao and S. H. Xia, *J. Phys. Chem. B*, 2006, **110**, 15858-15863.
- 32 W. Y. Li; L. N. Xu and J. Chen, *Adv. Funct. Mater.*, 2005, **15**, 851-857.
- 33 Y. G. Li, B. Tan and Y. Y. Wu, *Nano Lett.*, 2008, **8**, 265-270.
- 34 K. M. Shaju, F. Jiao, A. Debart; P. G. Bruce, *Phys. Chem. Chem. Phys.*, 2007, **9**, 1837-1842.
- 35 a) X. W. Xie and W. J. Shen, *Nanoscale*, 2009, **1**, 50-60; b) Y. Lou, J. Ma, X. M. Cao, L. Wang, Q. G. Dai, Z. Y. Zhao, Y. F. Cai, W. C. Zhan, Y. L. Guo, P. Hu, G. Z. Lu and Y. Guo, *ACS Catal.*, 2014, **4**, 4143-4152.
- 36 L. F. Liotta, H. J. Wu, G. Pantaleoa and A. M. Venezia, *Catal. Sci. Technol.*, 2013, **3**, 3085-3102.
- 37 X. Wang, W. Zhong and Y. W. Li, *Catal. Sci. Technol.*, 2015, **5**, 1014-1020.
- 38 P. M. Kouotou, H. Vieker, Z. Y. Tian, P. H. Tchoua Ngamou, A. El Kasmi, A. Beyer, A. Götzhäuserb and K. Kohse-Höinghaus, *Catal. Sci. Technol.*, 2014, **4**, 3359-3367.
- 39 J. Li, G. Z. Lu, G. S. Wu, D. S. Mao, Y. L. Guo, Y. Q. Wang and Y. Guo, *Catal. Sci. Technol.*, 2014, **4**, 1268-1275.
- 40 Y. H. Teng, Y. Kusano, M. Azuma, M. Haruta and Y. Shimakawa, *Catal. Sci. Technol.*, 2011, **1**, 920-922.
- 41 T. He, D. R. Chen, X. L. Jiao, Y. L. Wang and Y. Z. Duan, *Chem. Mater.*, 2005, **17**, 4023-4030.
- 42 D. Axel, P. Michael, M. Jochen, E. Katrin, H. Andreas and P. Jutzi, *Eur. J. Inorg. Chem.*, 2012, 198-202.
- 43 J. S. Chen, T. Zhu, Q. H. Hu, J. J. Gao, F. B. Su, S. Z. Qiao and X. W. Lou, *ACS Appl. Mater. Interfaces*, 2010, **2**, 3628-3635.
- 44 E. D. Park and J. S. Lee, *J. Catal.* 1999, **186**, 1-11.
- 45 a) L. C. Wang, L. He, Y. M. Liu, Y. Cao, H. Y. He, K. N. Fan and J. H. Zhuang, *J. Catal.*, 2009, **264**, 145-153. b) X.T. Nie, H. F. Qian, Q. J. Ge, H. Y. Xu and R. C. Jin, *ACS Nano*, 2012, **6**, 6014-6022.
- 46 Y. B. Yu, T. Takei, H. Ohashi, H. He, X. L. Zhang and M. Haruta, *J. Catal.*, 2009, **267**, 121-128.
- 47 B. Sun, X. Z. Feng, Y. Yao, Q. Su, W. J. Ji and C. T. Au, *ACS Catal.*, 2013, **3**, 3099-3105.
- 48 Y. Yao, Q. Su, X. Z. Feng, B. Sun, W. J. Ji and C. T. Au, *Catal. Sci. Technol.*, 2015, **5**, 1065-1075.
- 49 D. Briggs and M. P. Seah (Eds), *Practical Surface Analysis (2nd Edition)*, Wiley, Chichester, 1990.
- 50 D. A. Shirley, *Phys. Rev. B*, 1972, **5**, 4709.
- 51 a) S. Tougaard, *Surface Science*, 1989, **216**, 343-360. b) S. Tougaard, *J. Electron Spectrosc. Relat. Phenom.*, 1990, **52**, 243-271. c) S. Hansen and S. Tougaard, *Surf. Interface Anal.*, 1991, **17**, 593-607.
- 52 X. Wang, X. Y. Chen, L. S. Gao, H. G. Zheng, Z. D. Zhang and Y. T. Qian, *J. Phys. Chem. B*, 2004, **108**, 16401-16404.
- 53 M. Valden, X. Lai and D. W. Goodman, *Science*, 1998, **281**, 1647-1650.
- 54 G. Patrick, E. van der Lingen, C. W. Corti, R. J. Holliday and D. T. Thompson, *Top. Catal.*, 2004, **30-31**, 273-279.
- 55 M. Date, M. Okumura, S. Tsubota and M. Haruta, *Angew. Chem. Int. Ed.*, 2004, **43**, 2129-2132.
- 56 a) W. S. Epling, G. B. Hoflund, J. F. Weaver, S. Tsubota and M. Haruta, *J. Phys. Chem.*, 1996, **100**, 9929-9934. b) B. Shen, T. Liu, N. Zhao, X. Yang and L. Deng, *J. Environ. Sci.*, 2010, **22**, 1447-1454. c) J. Li, G. Z. Lu, G. S. Wu, D. S. Mao, Y. L. Guo, Y. Q. Wang and Y. Guo, *Catal. Sci. Technol.*, 2014, **4**, 1268-1275. d) B. Y. Bai and J. H. Li, *ACS Catal.*, 2014, **4**, 2753-2762. e) Y. X. Liu, H. X. Dai, J. G. Deng, S. H. Xie, H. G. Yang, W. Tan, W. Han, Y. Jiang, G. S. Guo, *J. Catal.* 2014, **309**, 408-418.
- 57 Z. Y. Fei, B. Sun, L. Zhao, W. J. Ji and C. T. Au, *Chem. Eur. J.*, 2013, **19**, 6480-6487.
- 58 D. Widmann, R. Leppelt and R. J. Behm, *J. Catal.*, 2007, **251**, 437-442.
- 59 Z. Y. Duan and G. Henkelman, *ACS Catal.*, 2015, **5**, 1589-1595.
- 60 K. Omata, T. Takada, S. Kasahara and M. Yamada, *Appl. Catal. A*, 1996, **146**, 255-267.
- 61 J. Jansson, *J. Catal.*, 2000, **194**, 55-60.
- 62 J. Jansson, M. Skoglundh, E. Fridell and P. Thormählen, *Top. Catal.*, 2001, **16/17**, 385-389.

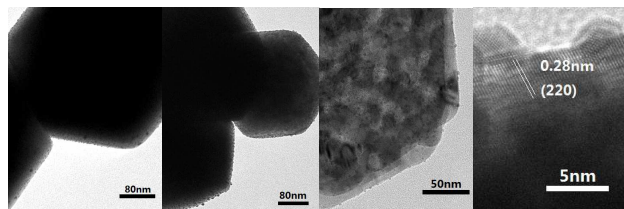
- 63 J. Jansson, A.E.C. Palmqvist, E. Fridell, M. Skoglundh, L. Öterlund, P. Thormählen and V. Langer, *J. Catal.*, 2002, **211**, 387-397.
- 64 F. Grillo, M. M. Natile and A. Glisenti, *Appl. Catal. B: Environ.*, 2004, **48**, 267-274.
- 65 a) K. Qian, L. F. Luo, H. Z. Bao, Q. Hua, Z. Q. Jiang and W. X. Huang, *Catal. Sci. Technol.*, 2013, **3**, 679-687; b) S. L. Chen, L. F. Luo, Z. Q. Jiang and W. X. Huang, *ACS Catal.*, 2015, **5**, 1653-1662.
- 66 D. C. Meier, X. F. Lai and D. W. Goodman, in "Surface Chemistry and Catalysis" (Eds.: A. F. Carley, P. R. Davies, G. J. Hutchings and M. S. Spencer), Kluwer/Plenum, New York, 2002, pp. 147-189.
- 67 Y. X. Liu, H. X. Dai, J. G. Deng, S. H. Xie, H. G. Yang, W. Tan, W. Han, Y. Jiang and G. S. Guo, *J. Catal.*, 2014, **309**, 408-418.
- 68 Y. G. Li, L. P. Zhu, Y. M. Guo, J. Jiang, L. Hu, Z. Wen, L. W. Sun and Z. Z. Ye, *ChemCatChem*, 2013, **5**, 3576-3581.
- 69 R. S. Drago, K. Jurczyk, D. J. Singh and V. Young, *Appl. Catal. B.*, 1995, **6**, 155-168.

Table of Contents

Enhanced Low Temperature CO Oxidation by Pretreatment: Specialty of the Au-Co₃O₄ Oxide Interfacial Structures

*Y. Yao, L. L. Gu, W. Jiang, H. C. Sun, Q. Su, J. Zhao, W. J. Ji, * and C. T. Au **

The enhanced CO oxidation by Au deposition and particularly He- and in situ-pretreatments has been elucidated in light of the structural specialties associated with the facets of Co₃O₄ substrates and the corresponding Au-Co₃O₄ interfaces.



Pretreatment enhanced CO oxidation:

Co₃O₄ substrates: (001) > (112) > (111)

Au-Co₃O₄ interfaces: Au/(112) > Au/(001) > Au/(111)

GHSV = 30,000 ml h⁻¹ g⁻¹, CO/O₂/N₂ = 1.6:21:77.4 (v/v/v)